Unified plate finite elements for the large strain analysis of hyperelastic material structures

International Journal of Non-Linear Mechanics 155 (2023) 104465

Contents lists available at ScienceDirect

International Journal of Non-Linear Mechanics

journal homepage: www.elsevier.com/locate/nlm

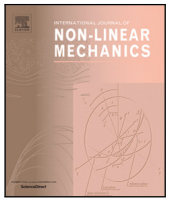

Unified plate finite elements for the large strain analysis of hyperelastic material structures

R. Augello, E. Carrera, M. Filippi, A. Pagani *, E. Tortorelli

Mul² Lab, Department of Mechanical and Aerospace Engineering, Politecnico di Torino, Corso Duca degli Abruzzi 24, 10129 Torino, Italy

ARTICLE INFO

Keywords:
High-order finite elements
Plates
Soft matter
Nearly incompressible hyperelastic materials
First-invariant hyperelasticity

ABSTRACT

This paper proposes a high-order two-dimensional (2D) finite element model for the analysis of isotropic, nearly incompressible hyperelastic material structures based on a decoupled Neo–Hookean strain energy function. The model is based on the Carrera Unified Formulation (CUF) , which allows to automatically implement different kinematics by using an opportune recursive notation. The principle of virtual work and a finite element approximation are exploited to obtain the nonlinear governing equations. Considering the three-dimensional full Green–Lagrange strain components and given the material Jacobian tensor, the explicit forms of tangent stiffness matrices of unified plate elements are presented in terms of the fundamental nuclei, which are independent of the theory approximation order. Several problems of soft material plates under uniform pressure are investigated, including a silicone rubber clamped plate and a simply supported plate made of biological material. The proposed model is compared with literature results including those coming from experiments and numerical solutions. The numerical investigation demonstrated the validity and accuracy of the proposed methodology for the analysis of hyperelastic plates.

1. Introduction

Structures made of hyperelastic soft materials are widely used in different engineering fields, from aerospace to biomedical. Some examples are represented by neurosurgery in the biomedical field [1], in the diagnosis of breast cancer by differentiating healthy tissues from diseased ones [2], and in the description of the behaviour of the arteries [3,4]. In the mechanical and aerospace fields, hyperelastic materials are exploited to produce devices characterized by unique elastic properties, such as pressure sensors [5], optical composites used for optical transmittance [6], devices that exploit Soft Electroactive Materials (SEAM) for conversion of mechanical energy into electrical energy such as Wave Energy Converter (WEC) able to convert wave energy into electrical energy through a membrane of dielectric material [7,8]. From a physical point of view, structures can undergo large deformations where the elastic constitutive equations lose validity. In addition, some structures have a very small linear region of the constitutive model, thus they have nonlinear behaviour.

In these years, researchers developed different strain energy function models to describe the strong nonlinear behaviour that this type of structures usually show during services. The most used model is the Neo–Hookean one. It derives from the molecular theory that the measured material is modelled as a network of a long chain of molecules that are bound at a few points. Therefore, the elastic energy of the network will be the sum of the energies of the individual chains [9]. Another polynomial strain energy function is the Mooney–Rivlin model, described by Mooney and Rivlin expressed in terms of the Cauchy–Green deformation tensor invariants [10]. This model was used for describing the behaviour of porcine brain tissue [11]. The Ogden model was developed in 1972 [12] and it is mainly used today to fit brain tissue test data as described by Kaster [1]. Moreover, Saccomandi et al. [13] discussed the significant impact that the Ogden model has had on the field of rubber mechanics and nonlinear elasticity over the past 50 years, and its continued relevance and importance in these fields today. The models previously described have polynomial forms of the strain energy functions. They are mainly used for biological tissue because of their simplicity. Instead, the Gent model has a logarithmic form and was proposed by Gent in 1996 [14]. This model reproduces accurately the behaviour of many new elastomeric and biological materials as studied by Horgan [15]. In [16], key features of the Gent model are discussed, including its simplicity, its ability to accurately describe the behaviour of rubber materials under various deformation conditions, and its ability to be extended to model other materials as well. More details and other material models are described by Khaniki et al. [17]. In this work, considered problems refer to a Neo–Hookean model. The reference solution of Breslavsky is also obtained using a Neo–Hookean model [18,19]. Instead, the reference solution of a silicone rubber plate by Amabili refers to a Mooney–Rivlin model [20]. It is important to employ an appropriate strain energy

* Corresponding author.
E-mail address: alfonso.pagani@polito.it (A. Pagani).

https://doi.org/10.1016/j.ijnonlinmec.2023.104465
Received 21 March 2023; Received in revised form 24 May 2023; Accepted 7 June 2023
Available online 13 June 2023

function to model the structures. In the work of Khaniki et al. [21] structures related to biological materials of the human body such as the brain, arteries, skeletal muscles, skin, adipose tissue, and problems related to polymeric structures in different mechanical conditions are investigated.

The nonlinear analysis of nearly incompressible hyperelastic materials presents some difficulties because the bulk modulus has orders of magnitude larger than the shear modulus. Among the main issues, there are instabilities and phenomena of locking. Many researchers have tried to overcome these shortcomings. For example, in the work of Sussman and Bathe [22] a finite element formulation was presented for the analysis with both geometrical and physical nonlinearities of compressible and incompressible solids. Babuška and Suri investigated Poisson locking using the standard formulation, also called the displacement formulation [23]. In the early work of Babuška [24], they also investigated shear and membrane locking when the thickness of the plate or shell is very small. Other works, however, considered mixed formulations such as that of Caylak and Mahnken [25]. Düster et al. [26] applied p-FEM to finite isotropic hyperelastic bodies. These last two works are mainly based on the method $\bar{\boldsymbol{F}}$, in which the deformation gradient is divided into two parts, isochoric and dilatational.

After discussing the issues related to the nonlinear analysis structures in hyperelastic material, it is important to develop simple and accurate models for 1D and 2D cases. Many works proposed these models. For example, Chen and Wang [27] developed a model where the Yeoh governing equations of a hyperelastic beam are shown using the principle of the minimum energy potential. In 2D case, both Chen [28] and Breslavsky [18,19] analysed the static behaviour of thin plates of Neo–Hookean and Mooney–Rivlin material. In addition, Amabili [20] studied the behaviour of a silicone plate and compared the solution with experimental data. The equations of motion have been obtained by a unified energy approach, and geometrical nonlinearities are modelled according to the Novozhilov nonlinear shell theory. Amabili et al. [29] also developed a geometrically nonlinear theory for circular cylindrical shells made of incompressible hyperelastic materials using a 9-parameter higher-order theory. Verhelst et al. [30] presented formulations of stretch-based material models for isogeometric Kirchhoff–Love shells. They verified formulations on invariant-based Neo–Hookean and Mooney–Rivlin models using several numerical benchmarks. A numerical solution technique, named as variational differential quadrature (VDQ), was adopted for the compressible nonlinear elasticity problems by Hassani et al. [31].

The present work aims at introducing a unified 2D element able to deal with the nonlinear analysis of hyperelastic materials. The model is built in the framework of the Carrera Unified Formulation (CUF) which allows for the development of a plate finite element (FE) with different kinematics, from low- to higher-order. The FE arrays are written in terms of fundamental nuclei, which are invariant of the theory approximation order, and therefore the equations can be written in the compact form [32–34]. Recently, CUF was introduced to deal with a one-dimensional finite element for the analysis of hyperelastic soft materials [35]. Here, the formulation is further extended to deal with hyperelastic plates. This paper is structured as follows: a description of hyperelastic materials models and strain energy function considered in Section 2; CUF and finite element method for 2D models in Section 3; governing equations in the unified form and Newton–Raphson method are described in Section 4; then, numerical results are discussed in Section 5; finally, the main conclusions are drawn.

2. Nearly incompressible isotropic hyperelastic materials

2.1. Strain energy function

In this paper, homogeneous materials are considered, thus the strain energy function, Ψ, only depends on the strain gradient tensor, $\boldsymbol{F}$. For isotropic hyperelastic materials, Ψ can be expressed in terms of principal stretches (λ_1, λ_2, λ_3), which are the eigenvalues of $\boldsymbol{F}$. The energy function Ψ can also be defined as a function of the invariants (I_1, I_2, I_3) of the right Cauchy–Green strain tensor, defined as follows:

$$\boldsymbol{C} = \boldsymbol{F}^T \boldsymbol{F}. \tag{1}$$

It is possible to write:

$$\Psi = \Psi(I_1, I_2, I_3) \tag{2}$$

where

$$\begin{aligned} I_1 &= \mathrm{tr}(\boldsymbol{C}) \\ I_2 &= \frac{1}{2}(I_1^2 - \mathrm{tr}(\boldsymbol{C}^2)) \\ I_3 &= \det(\boldsymbol{C}) \end{aligned} \tag{3}$$

and tr(•) and det(•) represent the trace and determinant of a tensor, respectively.

In the case of a nearly incompressible model, the Jacobian determinant $J = \det(\boldsymbol{F})$ represents the volume ratio, and hence the value of I_3 is approximately equal to the unit.

With a thermodynamic similarity, as described by Flory [36], the tensor $\boldsymbol{F}$ can be written by dividing it into two parts: $\boldsymbol{F}_{\mathrm{vol}} = J^{\frac{1}{3}}\mathbf{1}$ and $\overline{\boldsymbol{F}} = J^{-\frac{1}{3}}\boldsymbol{F}$ representing the volumetric part, related to deformation, and the isochoric part, respectively. Introducing Eq. (1), it is possible to write $\boldsymbol{C}_{\mathrm{vol}} = J^{\frac{2}{3}}\mathbf{1}$ and $\overline{\boldsymbol{C}} = J^{-\frac{2}{3}}\boldsymbol{C}$, and to obtain $\boldsymbol{C} = \boldsymbol{C}_{\mathrm{vol}}\overline{\boldsymbol{C}}$. Now, the strain energy function can be decoupled into its volumetric (U) and isochoric ($\bar{\Psi}$ part):

$$\Psi = U(J) + \overline{\Psi}(\overline{I_1}, \overline{I_2}) \tag{4}$$

where $\overline{I_1}$, $\overline{I_2}$ are the invariants of the isochoric part of the right Cauchy–Green strain tensor, $\overline{\boldsymbol{C}}$. The function $U(J)$ acts as a penalty of incompressibility, and it must be strictly convex, twice differentiable and continuous [37]. In the literature, several formulas [38] exist to express such a function, and in this work, we use the one proposed by Sussman and Bathe [22], where:

$$U(J) = \frac{1}{D_1}(J-1)^2 \tag{5}$$

where $D_1 = 2/k$ is the incompressibility material parameter and k is the bulk modulus.

In the literature, there are many definitions of the isochoric part of the strain energy function $\bar{\Psi}$ [15,39]. The most commonly used, often for biological materials, are classified with respect to the form of the equation, the number of strain invariants used and the ability to fit experimental data [9]. Polynomial forms of strain energy functions are the most used due to their simplicity and efficiency. In this paper, a Neo–Hookean model is used and the strain energy function is related only to the first invariant such that $\bar{\Psi} = \bar{\Psi}(\bar{I}_1)$. In particular, it assumes the following form:

$$\overline{\Psi}(\overline{I_1}) = \frac{\mu}{2}\left(\overline{I_1} - 3\right) \tag{6}$$

where μ is the shear modulus for infinitesimal deformations.

2.2. The Jacobian tensor

The constitutive relation in its general form is represented by the second stress tensor Piola–Kirchhoff (PK-2) defined as:

$$\boldsymbol{S} = 2\frac{\partial \Psi}{\partial \boldsymbol{C}} \tag{7}$$

Introducing Eq. (4) into Eq. (7), th PK-2 stress tensor can be written as the sum of a volumetric and an isochoric part:

$$\begin{aligned} \boldsymbol{S} &= \boldsymbol{S}^{\mathrm{vol}} + \boldsymbol{S}^{\mathrm{iso}} \\ \boldsymbol{S}^{\mathrm{vol}} &= J\, p\, \boldsymbol{C}^{-1} \\ \boldsymbol{S}^{\mathrm{iso}} &= 2\, J^{-\frac{2}{3}} \frac{\partial \overline{\Psi}}{\partial \overline{I_1}} \left(\mathbf{1} - \frac{1}{3}\overline{I_1}\,\boldsymbol{C}^{-1}\right) \end{aligned} \tag{8}$$

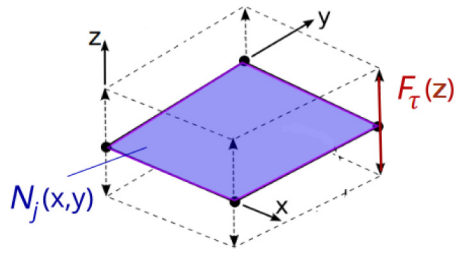

Fig. 1. CUF-FEM configuration for plate model.

Where $\mathbf{1}$ represents the unit matrix, $\boldsymbol{C}^{-1}$ is the inverse of the Cauchy–Green tensor, and $p = \frac{U}{J}$ is the hydrostatic pressure. The isochoric contribution $\boldsymbol{S}_{iso}$ refers to hyperelastic models correlated to the first invariant.

Consider PK-2 $\boldsymbol{S}$ of one point at some time t. According to Holzapfel [40], $\boldsymbol{S}$ can be evaluated as a function of a variable which can be assumed as $\boldsymbol{C}$. It is possible to write a linear relationship between the increments of $\boldsymbol{S}$ and C:

$$\Delta \boldsymbol{S} = \boldsymbol{C} \cdot \frac{1}{2} \Delta \boldsymbol{C} \tag{9}$$

where $\boldsymbol{C}$ is the gradient of the function $\boldsymbol{S}$. This quantity is the fourth-order elasticity tensor (*Jacobian tensor*) and measures the change in stresses starting from the change in strain and is defined as:

$$\boldsymbol{C} = \frac{\partial \boldsymbol{S}}{\partial \boldsymbol{E}} = 2\frac{\partial \boldsymbol{S}}{\partial \boldsymbol{C}} = 4\frac{\partial^2 \Psi}{\partial \boldsymbol{C} \partial \boldsymbol{C}} \tag{10}$$

where $\boldsymbol{E} = \frac{1}{2}(\boldsymbol{C} - \mathbf{1})$ is the Green–Lagrange strain tensor. Considering $U = U(J)$ and $\overline{\Psi} = \overline{\Psi}(\overline{I}_1)$ and introducing the Eqs. (8) and (10) it is possible to get the expression of the material Jacobian tensor:

$$\boldsymbol{C} = \boldsymbol{C}^{\text{vol}} + \boldsymbol{C}^{\text{iso}} \tag{11}$$

A detailed description is shown in [35,40].

3. Two-dimensional finite elements

The two-dimensional (2D) model adopted in this work is based on the Carrera Unified Formulation (CUF) [32,33]. CUF allows writing the equations of any refined theory 1D, 2D, or 3D in terms of a few fundamental nuclei FNs, whose shape does not depend on the assumptions used, such as type and order of the function, to describe the field of displacements.

Referring to Fig. 1, the three-dimensional (3D) displacement field $\boldsymbol{U}(x, y, z)$ can be expressed as a product between a 2D in-plane shape function $N_i(x, y)$ and 1D expansion function $F_\tau(z)$.

$$\boldsymbol{U}(x, y, z) = F_\tau(z) N_i(x, y) \boldsymbol{q}_{\tau i}, \qquad \tau = 1, \dots, M \qquad i = 1, \dots, p+1 \tag{12}$$

where $F_\tau(z)$ is the function of expansion along the thickness, with M equal to the number of terms of the expansion, $q_{\tau i}$ are the discrete nodal displacements, $N_i(x, y)$ are the 2D shape functions to use for the finite element method in the plane xy of the mean surface, p denotes the order of the shape functions and the repeated index i indicates summation. Note that the choice of the function F_τ is made a priori and is completely arbitrary but its choice characterizes the model adopted. According to Pagani e Carrera [41], it is possible to write the Green–Lagrange strain vector as:

$$\boldsymbol{E} = (\boldsymbol{b}_l + \boldsymbol{b}_{nl})\boldsymbol{U} = (\boldsymbol{b}_l + \boldsymbol{b}_{nl}) F_\tau(z) N_i(x, y) \boldsymbol{q}_{\tau i} = (\boldsymbol{B}_l^{\tau i} + \boldsymbol{B}_{nl}^{\tau i}) \boldsymbol{q}_{\tau i} \tag{13}$$

where $\boldsymbol{B}_l^{\tau j}$ and $\boldsymbol{B}_{nl}^{\tau j}$ are the matrices of derivative operators applied to the form functions in the linear and nonlinear case, respectively. In this paper, Lagrange Expansion (LE) models are used as expansion functions $F_\tau(z)$. For simplicity, the considered plate theories are indicated by the acronym LDN, which represents the Layer-wise Displacement-based theory with the order of expansion N [34]. Specifically, the two-node linear (LD1) and three-node quadratic (LD2) have been developed along the thickness of plates. For 2D in-plane shape functions $N_i(x, y)$, four-node bilinear (Q4) and nine-node quadratic (Q9) have been adopted. Note that the choice of discretization along the thickness is independent of the choice of discretization in the xy plane.

4. Governing equations

4.1. Tangent stiffness matrix

In this section, the tangent stiffness matrix is defined. It is used in the interactions of Newton–Raphson method. Starting from the CUF-FEM formulation and considering a generic expansion for a 2D element, it is possible to define the tangent stiffness matrix for hyperelastic materials. As already described, the strain vector can be written in terms of the unknowns generalized nodal displacements. In this case, $\boldsymbol{E}$ is the strain vector derived from the Green–Lagrange strain tensor and $\boldsymbol{U}_{\tau i}$ is the nodal virtual displacements. Therefore, it is possible to write:

$$\boldsymbol{E} = (\boldsymbol{b}_l + \boldsymbol{b}_{nl})\boldsymbol{u} = (\boldsymbol{b}_l + \boldsymbol{b}_{nl}) F_\tau(x, z) N_i(y) \boldsymbol{U}_{\tau i} = (\boldsymbol{B}_l^{\tau i} + \boldsymbol{B}_{nl}^{\tau i}) \boldsymbol{U}_{\tau i} \tag{14}$$

Then the virtual variation is:

$$\delta \boldsymbol{E} = \delta((\boldsymbol{B}_l^{\tau i} + \boldsymbol{B}_{nl}^{\tau i})\boldsymbol{U}_{sj}) = (\boldsymbol{B}_l^{sj} + 2\boldsymbol{B}_{nl}^{sj})\delta \boldsymbol{U}_{sj} \tag{15}$$

where indexes τ and i have been respectively substituted with s and j for sake of convenience. The equilibrium equation must be linearized to obtain the expression of the fundamental nuclei of the tangent stiffness matrix.

$$\delta(\delta L_{int}) = \int_\Omega \delta(\delta \boldsymbol{E}^T \boldsymbol{S}) dV = \int_\Omega \delta \boldsymbol{E}^T \delta \boldsymbol{S} dV + \int_\Omega \delta(\delta \boldsymbol{E}^T) \boldsymbol{S} dV \tag{16}$$

The first right-hand side term corresponds to the linearization of the constitutive equation of hyperelastic materials. Holzapfel [40] adopted the formulation with first invariant:

$$\delta \boldsymbol{S} = \boldsymbol{C}\frac{1}{2}\delta \boldsymbol{C} = \boldsymbol{C}\delta \boldsymbol{E} = \boldsymbol{C}(\boldsymbol{B}_l^{sj} + 2\boldsymbol{B}_{nl}^{sj})\delta \boldsymbol{U}_{\tau i} \tag{17}$$

where $\boldsymbol{C}$ represents the tangent fourth-order elasticity tensor described in previous section. It is possible to write the linearization of the constitutive law in a weak form:

$$\begin{aligned}
\int_\Omega \delta \boldsymbol{E}^T \delta \boldsymbol{S} dV &= \int_\Omega \delta \boldsymbol{U}_{sj}^T (\boldsymbol{B}_l^{sj} + 2\boldsymbol{B}_{nl}^{sj})^T \boldsymbol{C} (\boldsymbol{B}_l^{\tau i} + 2\boldsymbol{B}_{nl}^{\tau i}) \delta \boldsymbol{U}_{\tau i} dV \\
&= \delta \boldsymbol{U}_{sj}^T \left[\int_\Omega \boldsymbol{B}_l^{sjT} \boldsymbol{C} \boldsymbol{B}_l^{\tau i} dV \right] \delta \boldsymbol{U}_{\tau i} \\
&\quad + \delta \boldsymbol{U}_{sj}^T \left[2\int_\Omega \boldsymbol{B}_l^{sjT} \boldsymbol{C} \boldsymbol{B}_{nl}^{\tau i} dV \right] \delta \boldsymbol{U}_{\tau i} + \\
&+ \delta \boldsymbol{U}_{sj}^T \left[2\int_\Omega \boldsymbol{B}_{nl}^{sjT} \boldsymbol{C} \boldsymbol{B}_l^{\tau i} dV \right] \delta \boldsymbol{U}_{\tau i} \\
&\quad + \delta \boldsymbol{U}_{sj}^T \left[\int_\Omega 2\boldsymbol{B}_l^{sjT} \boldsymbol{C} 2\boldsymbol{B}_l^{\tau i} dV \right] \delta \boldsymbol{U}_{\tau i}
\end{aligned} \tag{18}$$

Four contributions of 3×3 matrices are defined:

$$\begin{aligned}
\boldsymbol{K}_{ll}^{ij\tau s} &= \int_\Omega \boldsymbol{B}_l^{sjT} \boldsymbol{C} \boldsymbol{B}_l^{\tau i} dV \\
\boldsymbol{K}_{lnl}^{ij\tau s} &= \int_\Omega \boldsymbol{B}_l^{sjT} \boldsymbol{C} \boldsymbol{B}_{nl}^{\tau i} dV \\
\boldsymbol{K}_{nll}^{ij\tau s} &= \int_\Omega 2\boldsymbol{B}_{nl}^{sjT} \boldsymbol{C} \boldsymbol{B}_l^{\tau i} dV \\
\boldsymbol{K}_{nlnl}^{ij\tau s} &= \int_\Omega 2\boldsymbol{B}_l^{sjT} \boldsymbol{C} 2\boldsymbol{B}_l^{\tau i} dV
\end{aligned} \tag{19}$$

where $\boldsymbol{K}_{ll}^{ij\tau s}$ is the linear contribution and $\boldsymbol{K}_{T_1}^{ij\tau s} = 2\boldsymbol{K}_{lnl}^{ij\tau s} + \boldsymbol{K}_{nll}^{ij\tau s} + 2\boldsymbol{K}_{nlnl}^{ij\tau s}$ is the nonlinear contribution of the tangent stiffness matrix.

It is possible to rewrite the linearized constitutive equation as:

$$\int_\Omega \delta \boldsymbol{E}^T \delta \boldsymbol{S} dV = \delta \boldsymbol{U}_{sj}{}^T \boldsymbol{K}_{ll}{}^{ij\tau s} \delta \boldsymbol{U}_{\tau i} + \delta \boldsymbol{U}_{sj}{}^T \boldsymbol{K}_{T_1}{}^{ij\tau s} \delta \boldsymbol{U}_{\tau i} \tag{20}$$

The second right-hand side term of Eq. (16) corresponds to the linearization of geometric equations. Once the matrix of differential operators $\boldsymbol{B}_{nl}{}^*$ and the virtual variation of the deformations have been defined:

$$\delta(\delta \boldsymbol{E}) = \boldsymbol{B}_{nl}{}^* \begin{Bmatrix} \delta U_{x_{\tau i}} \delta U_{x_{sj}} \\ \delta U_{y_{\tau i}} \delta U_{y_{sj}} \\ \delta U_{z_{\tau i}} \delta U_{z_{sj}} \end{Bmatrix} \tag{21}$$

The second term becomes:

$$\begin{aligned} \int_\Omega \delta(\delta \boldsymbol{E}^T) \boldsymbol{S} dV &= \int_\Omega \begin{Bmatrix} \delta U_{x_{\tau i}} \delta U_{x_{sj}} \\ \delta U_{y_{\tau i}} \delta U_{y_{sj}} \\ \delta U_{z_{\tau i}} \delta U_{z_{sj}} \end{Bmatrix} (\boldsymbol{B}_{nl}{}^*)^T \boldsymbol{S} dV \\ &= \int_\Omega \delta \boldsymbol{U}_{sj}{}^T \ \mathrm{diag}((\boldsymbol{B}_{nl}{}^*)^T \boldsymbol{S}) \delta \boldsymbol{U}_{\tau i} dV \\ &= \delta \boldsymbol{U}_{sj}{}^T \boldsymbol{K}_\sigma{}^{ij\tau s} \delta \boldsymbol{U}_{\tau i} \end{aligned} \tag{22}$$

where $\boldsymbol{K}_\sigma{}^{ij\tau s}$ is the geometric stiffness matrix and derives from the linearization of the nonlinear displacement-strain relationship.

Then, substituting the different quantities in the Eq. (16), it is possible to obtain the fundamental nuclei of the tangent stiffness matrix as the sum of the linear, nonlinear and geometric contribution:

$$\begin{aligned} \delta(\delta L_{int}) &= \delta \boldsymbol{U}_{sj}{}^T \boldsymbol{K}_{ll}{}^{ij\tau s} \delta \boldsymbol{U}_{\tau i} + \delta \boldsymbol{U}_{sj}{}^T \boldsymbol{K}_{T_1}{}^{ij\tau s} \delta \boldsymbol{U}_{\tau i} + \delta \boldsymbol{U}_{sj}{}^T \boldsymbol{K}_\sigma{}^{ij\tau s} \delta \boldsymbol{U}_{\tau i} \\ &= \delta \boldsymbol{U}_{sj}{}^T \boldsymbol{K}_T{}^{ij\tau s} \delta \boldsymbol{U}_{\tau i} \end{aligned} \tag{23}$$

4.2. Internal force vector

Starting from the Eq. (15), the principle of virtual works establishes that:

$$\delta L_{\text{int}} - \delta L_{\text{est}} = 0 \tag{24}$$

Considering the Green–Lagrange strain $\boldsymbol{E}$ and stress tensors PK2 $\boldsymbol{S}$, the virtual variation of the work of the internal forces can be expressed as:

$$\delta L_{\text{int}} = \int_\Omega \delta \boldsymbol{E}^T \boldsymbol{S} dV \tag{25}$$

Now, adopting the same definition of generalized deformations and its virtual variation:

$$\delta \boldsymbol{E} = \delta(((\boldsymbol{B}_l{}^{\tau i} + \boldsymbol{B}_{nl}{}^{\tau i}) \boldsymbol{U}_{\tau i}) \boldsymbol{U}_{sj}) = (\boldsymbol{B}_l{}^{sj} + 2\boldsymbol{B}_{nl}{}^{sj}) \delta \boldsymbol{U}_{sj} \tag{26}$$

Substituting it in Eq. (25), it is possible to write:

$$\delta L_{\text{int}} = \int_\Omega \delta \boldsymbol{E}^T \boldsymbol{S} dV = \int_\Omega \delta \boldsymbol{U}_{sj}{}^T (\boldsymbol{B}_l{}^{sj} + 2\boldsymbol{B}_{nl}{}^{sj}) \boldsymbol{S} dV = \delta \boldsymbol{U}_{sj}{}^T \boldsymbol{F}_{int}{}^{sj} \tag{27}$$

The fundamental nuclei of the internal forces vector are obtained:

$$\boldsymbol{F}_{int}{}^{sj} = \int_\Omega (\boldsymbol{B}_l{}^{sj} + 2\boldsymbol{B}_{nl}{}^{sj}) \boldsymbol{S} dV \tag{28}$$

The FN of the external load vector is derived from the definition of 2D CUF-FEM. Considering p the vector of conservative loads, it is possible to write the virtual variation of the work done by external forces as:

$$\delta L_{\text{est}} = \int_\Omega \delta \boldsymbol{U}^T \boldsymbol{p} dV = \int_\Omega \boldsymbol{q}_{sj}{}^T F_s(z) N_j(x,y) \boldsymbol{p} dV = \boldsymbol{q}_{sj}{}^T \boldsymbol{p}_{sj} \tag{29}$$

Substituting in Eq. (24) and assembling the final structure, nonlinear algebraic equations are rewritten as:

$$\delta \boldsymbol{U} : \quad \boldsymbol{F}_{int} - \boldsymbol{F}_{ext} = 0 \tag{30}$$

Nonlinear equations are solved using the Newton–Raphson linearization . The vector of residual nodal forces $\boldsymbol{\varphi}_{res}$ can be linearized by Taylor series expansion introducing the tangent stiffness matrix $\boldsymbol{K}_T$. It is necessary to introduce a constraint relation to solve the equations. Different incremental schemes can be implemented using different constraint equation. A more detailed description of Newton–Raphson method is provided in Ref. [41]. In particular, the *arc-length* method provides a solution for nonlinear problems when critical points are present. This method is accurately described by Crisfield [42].

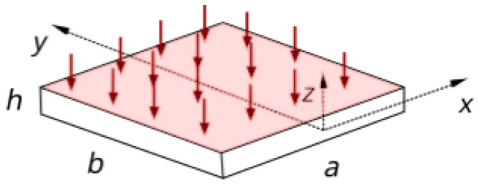

Fig. 2. Thin hyperelastic plate geometry under pressure.

Table 1
Material parameters of thin hyperelastic plate present in [19]. Neo–Hookean model adopted.

E	1247060.2 Pa
ν	0.4999
μ	415714.45 Pa
$D_1 = 2/k$	9.6226×10^{-10} Pa^{-1}

5. Numerical results

In this paper, three study cases taken from literature are analysed with the proposed 2D unified models:

- the first case refers to a simply supported square plate analysed with general Neo–Hookean material model and biological material model;
- the second case deals with a simply supported rectangular plate considering at first geometrical nonlinearities and then geometrical and physical nonlinearities;
- the last case refers to a clamped silicone rubber plate under uniform pressure.

All the cases consider to plates under pressure. A Neo–Hookean nearly incompressible material has been adopted.

5.1. Thin hyperelastic plate under pressure

The first case was considered by Breslavsky et al. in [19] using a incompressible model ($\nu = 0.5$). The same problem was analysed by Ansari et al. in [43] considering a nearly incompressible model. A simply supported plate is considered with $a = b = 0.1$ m, $h = 5 \times 10^{-4}$ m and it is subjected to uniform pressure with the following boundary conditions, Fig. 2:

$$w|_{\delta S} = M|_{\delta S} = u|_{\delta S} = v|_{\delta S} = 0 \tag{31}$$

where δS is the boundary plate.

In this work, we considered the nearly incompressible Neo–Hookean model with material parameters given in [19] and present in Table 1. In the xy plane, we used a number of elements of 8×8, 10×10 with four-nodes (Q4) and 10×10, 16×16 with nine-nodes (Q9). Along the thickness, however, it was sufficient to use a three-node quadratic Lagrangian expansion function (LD2) to obtain the accuracy of the solution. As shown in Fig. 3, for a few elements (in this case 8×8 Q4) the solution is not very accurate. Increasing the number of elements, however, the solution tends to coincide with the 27 degrees of freedom (DOF) Breslavsky solution obtained by the local model method, where the total number of degree of freedom DOF is given by $N = N_W + N_U + N_V$ [19]. Table 2 shows the centre point deformation

Table 2
Deflection measured at the centre of the thin hyperelastic plate for different FEM models. Comparison with 27 DOF solution in [19].

$p[kPa]$	w/h			Ref [19]
	8 × 8Q4	10 × 10Q4	10 × 10Q9	
0.029	6.848	9.030	9.043	10.109
0.285	17.741	19.318	19.226	20.132
1.917	37.642	38.912	39.192	39.980
4.292	54.337	55.052	56.075	57.020
8.019	76.571	76.935	78.601	80.032
10.476	91.047	91.854	93.243	94.984

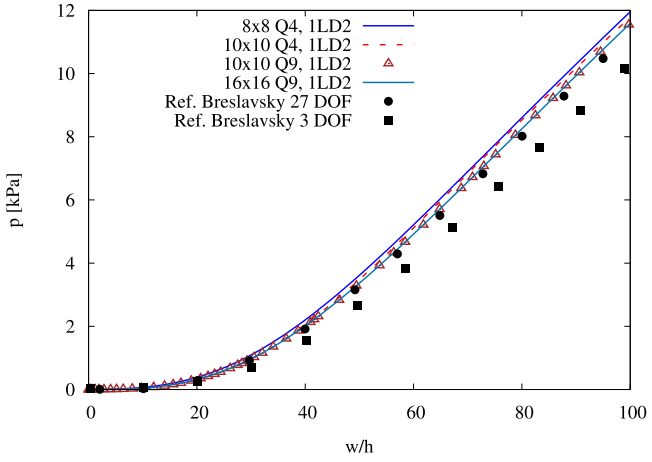

Fig. 3. Neo–Hookean plate pressure-deflection response. Deflection measured at the centre of the plate and normalized with respect to the plate thickness h. Comparison between different FEM models and solution with 27 DOF and 3 DOF of Breslavsky [19].

values for the different discretization models used and for different load steps. As it is possible to see from the graph, the convergence is achieved for a 10 × 10 Q9 mesh. Using the nearly incompressible model with $\nu = 0.4999$, it is possible to notice that it is almost coincident with the incompressible case. They are practically coincident for small deformations.

In Fig. 4, the pressure-deflection response of a thin plate is plotted using two different volumetric functions, $U_1 = \frac{1}{D_1}(J-1)^2$ and $U_2 = \frac{1}{D_1}(lnJ)^2$. As shown, the choice of volumetric function does not affect the results for a nearly incompressible material. It only could be detrimental or beneficial from the stability point of view.

5.2. Hyperelastic plate made of biological material

This case is also discussed by Breslavsky in [19]. The plate has the same dimensions and boundary conditions as in the previous example. The properties of the material are in [19] and they refer to the experimental data of the tunica adventitia of a human aorta available in [4]. A Neo–Hookean material model is considered with Young modulus $E = 59383.2$ Pa and it is considered the nearly incompressible material condition with $\nu = 0.4999$.

For convergence analysis, 4-node Q4 elements were used in the xy plane and a 3-node quadratic Lagrangian expansion (LD2) along the thickness. Various discretizations have been tested. From Fig. 5 it is possible to see that a small number of elements is already sufficient to obtain an accurate solution. Moreover, even if it was used a nearly incompressibility condition, the solution obtained is close to the solution of incompressible material (for small deformations it is nearly coincident) as shown in Table 3. Furthermore, this plate has identical dimensions to the previous case, yet there is a contrasting outcome concerning reference solutions due to varied material parameters.

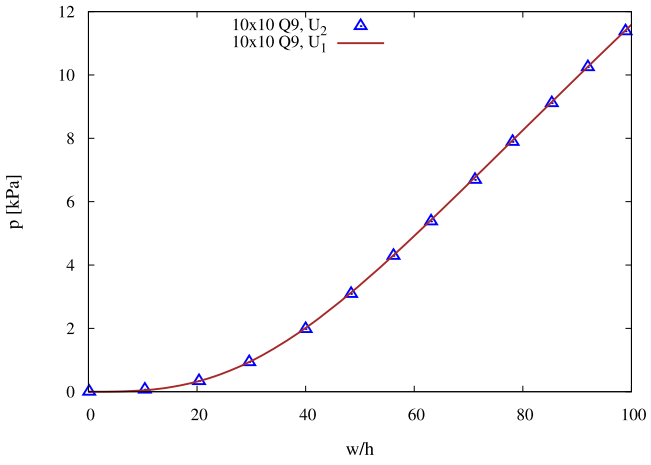

Fig. 4. Neo–Hookean plate pressure-deflection response. Deflection measured at the centre of the thin plate considering two different volumetric function U_1 and U_2.

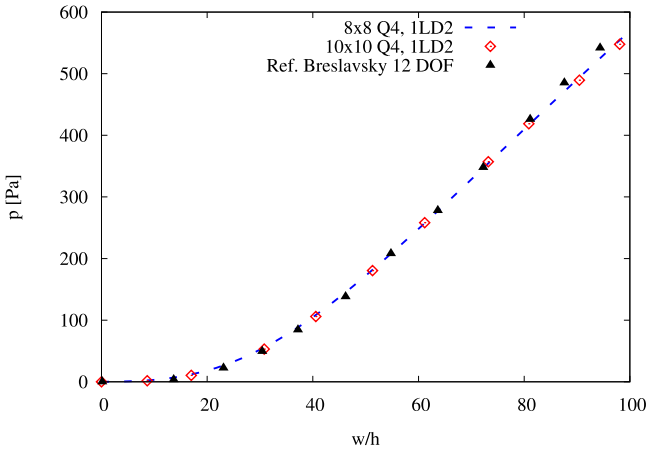

Fig. 5. Pressure load-middle point deflection response of the biological material plate. Comparison between two different numbers of element and solution with 12 DOF of Breslavsky [19].

Table 3
Middle point deflection of the biological material plate with mesh 8 × 8 Q4, 10 × 10 Q4 and Breslavsky's solution with 12 DOF [19] for various load levels.

$p[Pa]$	w/h		
	8 × 8Q4	10 × 10Q4	Ref. [19]
3.83	11.21	12.09	13.67
84.64	36.41	36.93	37.21
208.51	54.83	54.83	54.83
426.39	81.66	82.03	81.20
542.14	96.46	97.11	94.27
568.45	99.69	100.50	98.33

Specifically, the Young's modulus of the two cases differs by two orders of magnitude, resulting in a distinct value for D_1 and causing numerical complications in defining $U(J)$.

5.3. Rectangular plate: comparison between geometrical nonlinearities and geometrical and physical nonlinearities

The second example analysed is a simply supported rectangular plate, always subject to uniform pressure. In this case, the plate has the following dimensions: $a = 0.1$ m, $b = 0.12$ m and $h = 5 \times 10^{-4}$ m. The material properties considered are $E = 10^7$ Pa and $\nu = 0.4999$. The nearly incompressible material is considered. The analysed case

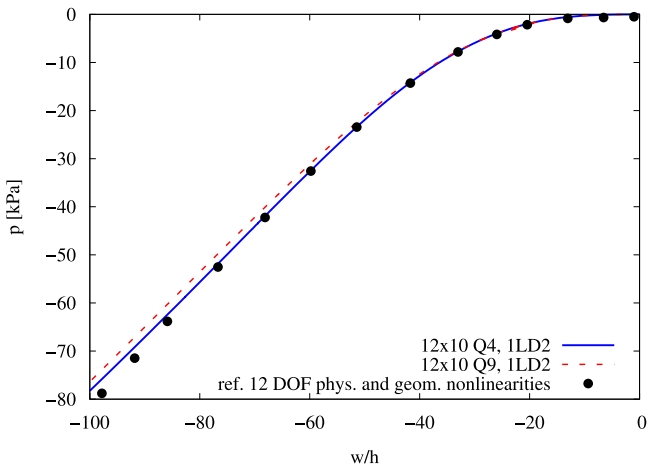

Fig. 6. Middle point deflection-pressure curves for models with geometrical and physical nonlinearities . Comparison between two different models 12×10 Q4, 12×10 Q9 and solution with 12 DOF of Breslavsky [18].

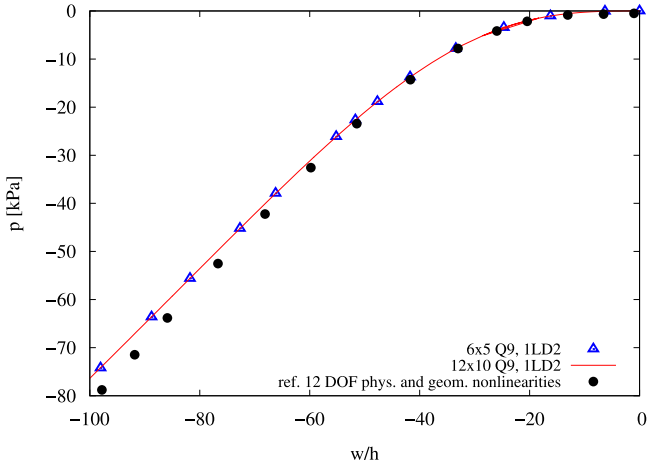

Fig. 7. Middle point deflection-pressure curves for models with geometrical and physical nonlinearity . Comparison between 6×5 Q9, 12×10 Q9 and solution with 12 DOF of Breslavsky [18].

is taken from Breslavsky et al. [18], where the incompressible model ($\nu = 0.5$) is used. For convergence analysis, a discretized model in the xy plane with 12×10 elements both Q4 and Q9 is investigated. From Fig. 6, the discretized model with nine-node elements presents a more accurate solution than four-nodes elements solution. In Fig. 7, another convergence analysis is investigated. The solutions with nine-nodes element Q9 and a different number of elements (6×5 and 12×10) are compared considering $\nu = 0.4999$. Note that a 6×5 Q9 mesh is already accurate enough to describe the behaviour of the plate made from material with almost incompressible Neo–Hookean condition. Finally, the model with 12×10 Q9 is assessed. The solution obtained considering only geometrical nonlinearities is compared with the solution obtained with both geometrical and physical ones. In Fig. 8, the solutions are similar to Breslavsky's solutions. In Fig. 9, undeformed configuration and deformed configuration with $p = 1.715,\ 8.694,\ 30.407$ kPa are shown. In addition, it is possible to see that a 3-node (quadratic) discretization model along the thickness is sufficient to obtain the accuracy of the results. Note that the solutions of the nearly incompressible are similar to the incompressible case and they coincide for small deformations.

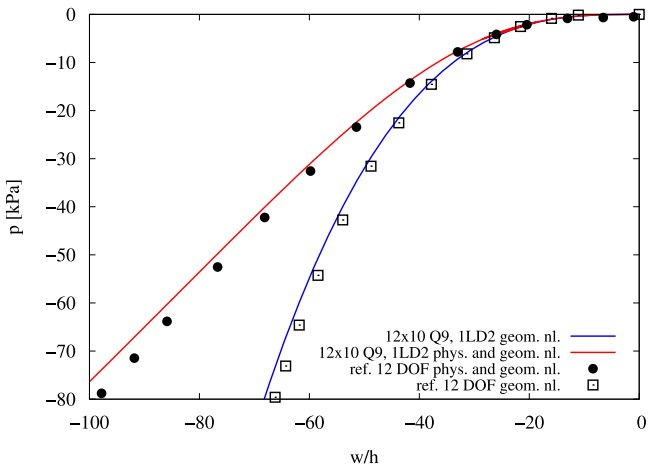

Fig. 8. Middle point deflection-pressure curves for 12×10 Q9 model and $\nu = 0.4999$. Comparison between solution with geometrical nonlinearities only and solution with both geometrical and physical nonlinearities . Comparison with 12 DOF Breslavsky's solution [18].

5.4. Silicone rubber plate

The last case under examination is taken from Amabili et al. [20]. In Fig. 10, a clamped plate with $a = b = 0.26$ m and thickness $h = 1.5 \times 10^{-3}$ m is shown. The silicone rubber plate is under aerostatic pressure and it has been investigated analytically, numerically, and experimentally, as shown in Fig. 11. The plate has the following boundary conditions:

$$w|_{\delta\Omega} = \frac{\partial w}{\partial \boldsymbol{n}}|_{\delta\Omega} = u|_{\delta\Omega} = v|_{\delta\Omega} = 0 \tag{32}$$

where $\partial\Omega$ is the plate's middle surface boundary and $\boldsymbol{n}$ is the normal to $\partial\Omega$ lying on the plate surface. In order to compare the experimental data with the numerical solution, the material parameters are obtained by a fitting procedure on the results of the uniaxial tension test. In [20], Amabili considered a Mooney–Rivlin material model with elastic strain energy function as $\bar{\Psi} = C_{10}(\bar{I}_1 - 3) + C_{01}(\bar{I}_2 - 3)$, where the two material parameters are $C_{10} = 253216$ Pa and $C_{01} = 470900$ Pa. In this paper, however, it is used a model of Neo–Hookean material dependent only on the first invariant, which is a special case of Mooney–Rivlin material [22]. Material parameters in Table 4 are considered where μ is the shear modulus, ν is the Poisson coefficient, D_1 is the material incompressibility parameter. Therefore, it was considered an almost incompressible model and it will be compared with the solution obtained by Amabili in the incompressible case ($\nu = 0.5$). For the convergence analysis, 4-node elements (Q4) and a different number of elements were used in the xy plane: 8×8, 10×10, 14×14, 18×18. Along the thickness, however, three-nodes are sufficient for the accuracy of the solution. As shown in Fig. 12 and Table 5, the configuration with fewer degrees of freedom stands between the reference numerical solution, where a 20×20 mesh was used, and the experimental solution. For the nearly incompressible Neo–Hookean model considered in this paper, the convergence is achieved with a 14×14 Q4 model and a quadratic Lagrange expansion function (LD2) along the thickness. The solution is practically coincident with the experimental solution in the case of small deformations, while for displacements $w > 35$ mm the solution slightly deviates from the FEM analysis carried out in [20]. Fig. 13 shows the undeformed and deformed states of the plate under two different load conditions.

6. Conclusions

This paper discussed two-dimensional (2D) high-order finite elements for the analysis of first-invariant hyperelastic Neo–Hookean

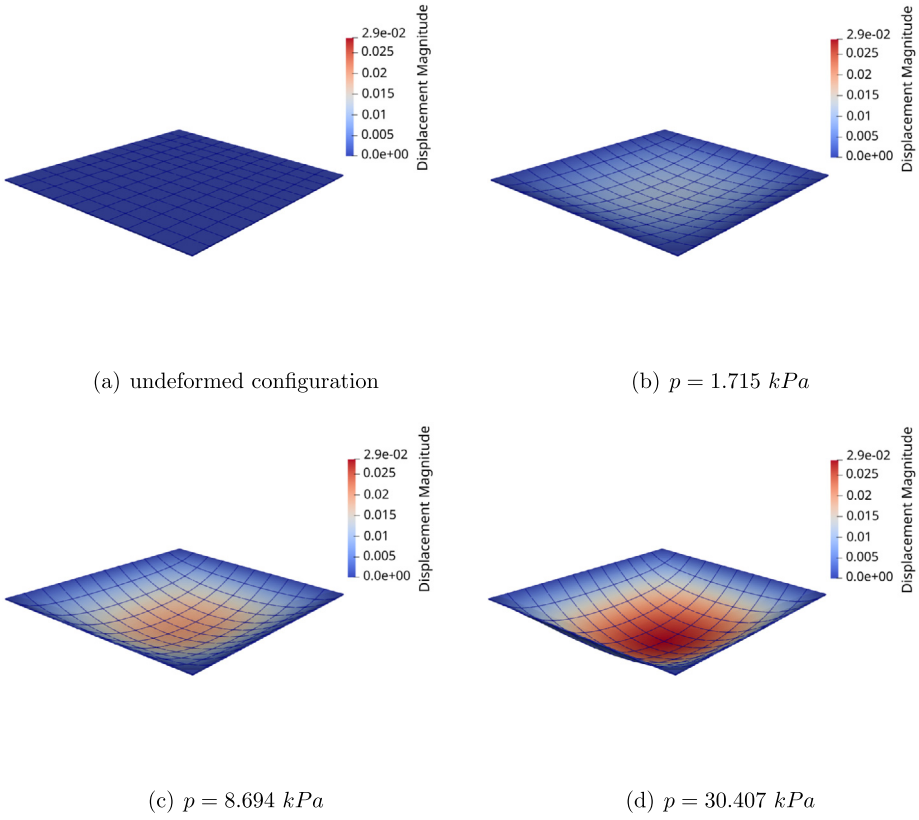

(a) undeformed configuration (b) $p = 1.715\ kPa$

(c) $p = 8.694\ kPa$ (d) $p = 30.407\ kPa$

Fig. 9. Undeformed and deformed states of the simply supported rectangular plate. 12 × 10 Q9 model.

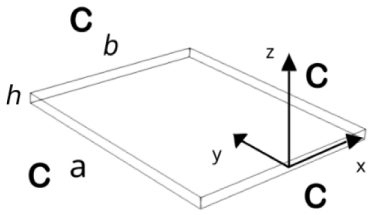

Fig. 10. Boundary condition and geometry of the silicone rubber plate.

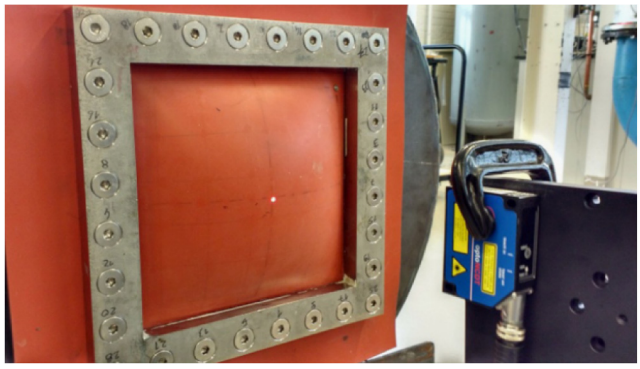

Fig. 11. Silicone rubber plate under a pressure of 1 Psi. The deflection at the centre point is measured using a Micro-Epsilon triangulation laser sensor [20].
Source: Adapted from [20] with permission from Elsevier.

Table 4
Material parameters of silicone rubber clamped plate (see Fig. 1 and Fig. 11) and subjected to uniform transverse pressure.

ν	0.4999
μ	$1.448 \times 10^6\ Pa$
$D_1 = 2/k$	$2.762 \times 10^{-10}\ Pa^{-1}$

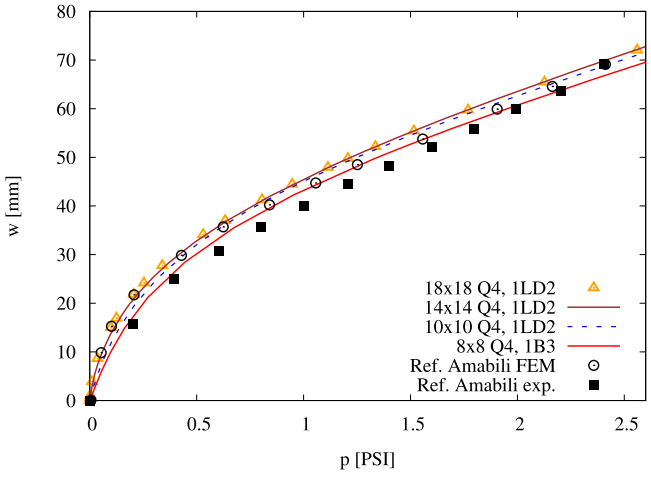

Fig. 12. Static deflection of the silicone plate measured at the centre as function of the pressure. Comparison between different FEM models and experimental and FEM solutions of Amabili et al. [20].

plates. According to the Carrera Unified Formulation (CUF), it is possible to write the governing equations in terms of a few fundamental nuclei (FNs), which are invariant of the theory approximation order. The strain energy function was decomposed and split into its volumetric and isochoric parts. The choice of the volumetric function does not affect the response of the nearly incompressible material, but it can only worsen or improve the locking phenomenon. Different problems

Table 5
Pressure-deformation values of the central point of the plate w/h for different mesh. Comparison with the reference solution in [20] of both FEM analysis and measured experimental data.

$p[Psi]$	w/h				
	8 × 8Q4	10 × 10Q4	14 × 14Q4	Ref. FEM	Ref. exp.
0.204	17.06	19.41	20.74	21.43	15.74
0.604	33.30	35.22	35.89	35.22	30.77
0.800	38.66	40.63	40.97	39.43	35.77
1.204	47.18	49.06	49.71	47.18	44.44
1.994	60.60	62.38	63.40	61.17	60.04

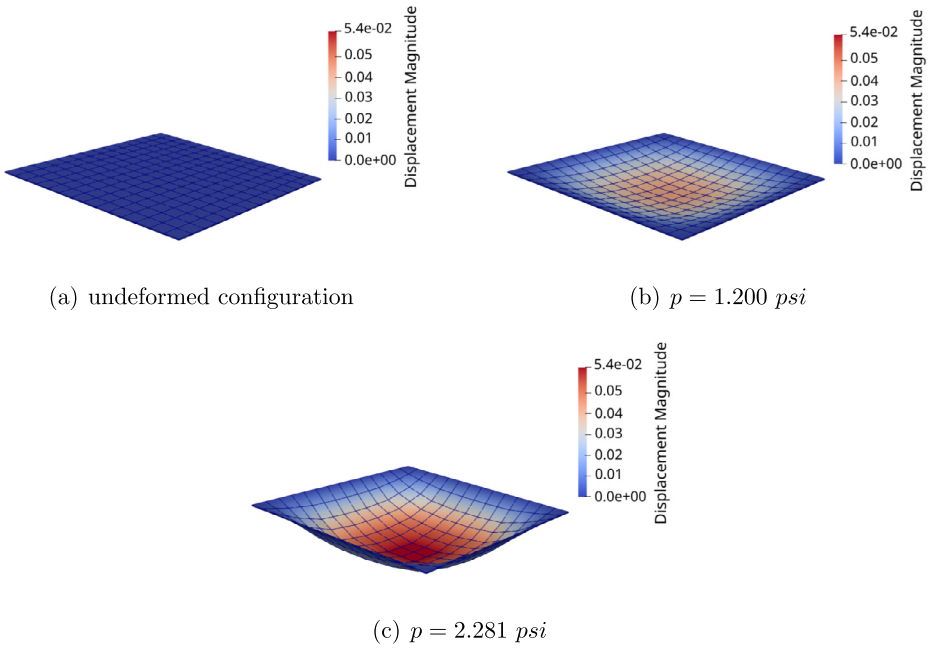

(a) undeformed configuration

(b) $p = 1.200\ psi$

(c) $p = 2.281\ psi$

Fig. 13. Undeformed and deformed states of the silicone rubber plate.

were considered and the effect of the theory approximation order on the convergence and the accuracy of the solutions is studied in detail. The numerical investigation has demonstrated:

- the validity and accuracy of the theory provided for plates with both geometrical and physical nonlinearities considering a nearly-incompressible Neo–Hookean model.
- the accuracy of the CUF-FEM methodology compared with experimental data for a clamped silicone rubber plate.
- a model with a three-node quadratic Lagrange expansion along the thickness correctly described the large deflection of thin plates under uniform pressure.
- the selection of the volumetric function has no impact on the response of the nearly incompressible material. It acts as a penalization of incompressibility.
- higher order model can help to overcome locking phenomena.

Based on the numerical results, there is sufficient confidence to support future developments in this area, such as the extension of this method to thick plates, where the only alternative is 3D elements. Furthermore, the proposed two-dimensional finite element method could be applied to model the behaviour of layerwise hyperelastic materials, which have unique mechanical properties due to their multi-layered structure. The research conducted provides enough confidence for future developments in this direction.

CRediT authorship contribution statement

R. Augello: Software, Validation, Investigation, Writing – review & editing. **E. Carrera:** Methodology, Resources, Supervision, Funding acquisition. **M. Filippi:** Software, Validation, Writing – review & editing. **A. Pagani:** Conceptualization, Methodology, Resources, Writing – review & editing, Supervision, Funding acquisition. **E. Tortorelli:** Formal analysis, Investigation, Writing – original draft, Visualization.

Declaration of competing interest

The authors declare that they have no known competing financial interests or personal relationships that could have appeared to influence the work reported in this paper.

Data availability

Data will be made available on request.

Acknowledgments

This study was carried out within the CNMS — Sustainable Mobility National Research Center and received funding from the European Union Next-GenerationEU (PIANO NAZIONALE DI RIPRESA E RESILIENZA (PNRR) — MISSIONE 4 COMPONENTE 2, INVESTIMENTO 1.4 — D.D. 1033 17/06/2022, CN00000023). This manuscript reflects only the authors' views and opinions, neither the European Union nor the European Commission can be considered responsible for them.

References

[1] T. Kaster, I. Sack, A. Samani, Measurement of the hyperelastic properties of ex vivo brain tissue slices, J. Biomech. 44 (6) (2011) 1158–1163.

[2] H. Mehrabian, A. Samani, An iterative hyperelastic parameters reconstruction for breast cancer assessment, in: X.P. Hu, A.V. Clough (Eds.), Medical Imaging 2008: Physiology, Function, and Structure from Medical Images, Vol. 6916, SPIE, International Society for Optics and Photonics, 2008, p. 69161C.
[3] M. Ahmadi, R. Ansari, Computational simulation of an artery narrowed by plaque using 3D FSI method: influence of the plaque angle, non-Newtonian properties of the blood flow and the hyperelastic artery models, Biomed. Phys. Eng. Express 5 (4) (2019) 045037.
[4] G.A. Holzapfel, Determination of material models for arterial walls from uniaxial extension tests and histological structure, J. Theoret. Biol. 238 (2) (2006) 290–302.
[5] A. Leber, A.G. Page, D. Yan, Y. Qu, S. Shadman, P. Reis, F. Sorin, Compressible and electrically conducting fibers for large-area sensing of pressures, Adv. Funct. Mater. 30 (2020) 1904274.
[6] F. López Jiménez, P. Upadhyaya, J. Liljenhjerte, P.M. Reis, S. Kumar, Soft optical composites for tunable transmittance, Extreme Mech. Lett. 9 (2016) 297–303.
[7] G. Moretti, G. Rosati, M. Righi, D. Forehand, D. Ingram, R. Vertechy, M. Fontana, Resonant wave energy harvester based on dielectric elastomer generator, Smart Mater. Struct. 27 (2018).
[8] G. Moretti, M. Santos Herran, M. Forehand, H. Jeffrey, R. Vertechy, M. Fontana, Advances in the development of dielectric elastomer generators for wave energy conversion, Renew. Sustain. Energy Rev. 117 (2020) 109430.
[9] C. Wex, S. Arndt, A. Stoll, C. Bruns, Y. Kupriyanova, Isotropic incompressible hyperelastic models for modelling the mechanical behaviour of biological tissues: A review, Biomed. Tech. Biomed. Eng. 60 (2015).
[10] R.S. Rivlin, Large elastic deformations of isotropic materials. IV. Further developments of the general theory, Philos. Trans. R. Soc. Lond. Ser. A Math. Phys. Eng. Sci. 241 (835) (1948) 379–397.
[11] B. Rashid, M. Destrade, M. Gilchrist, Mechanical characterization of brain tissue in simple shear at dynamic strain rates, J. Mech. Behav. Biomed. Mater. 28C (2013) 71–85.
[12] R.W. Ogden, Large deformation isotropic elasticity – on the correlation of theory and experiment for incompressible rubberlike solids, Proc. R. Soc. Lond. Ser. A Math. Phys. Eng. Sci. 326 (1567) (1972) 565–584.
[13] M. Destrade, L. Dorfmann, G. Saccomandi, The Ogden model of rubber mechanics: 50 years of impact on nonlinear elasticity, Phil. Trans. R. Soc. A 380 (2234) (2022) 20210332.
[14] A.N. Gent, A new constitutive relation for rubber, Rubber Chem. Technol. 69 (1) (1996) 59–61.
[15] C.O. Horgan, The remarkable Gent constitutive model for hyperelastic materials, Int. J. Non-Linear Mech. 68 (2015) 9–16, Mechanics of Rubber - in Memory of Alan Gent.
[16] G. Puglisi, G. Saccomandi, The Gent model for rubber-like materials: An appraisal for an ingenious and simple idea, Int. J. Non-Linear Mech. 68 (2015) 17–24, Mechanics of Rubber - in Memory of Alan Gent.
[17] H.B. Khaniki, M.H. Ghayesh, R. Chin, M. Amabili, A review on the nonlinear dynamics of hyperelastic structures, Nonlinear Dynam. 110 (2022).
[18] I.D. Breslavsky, M. Amabili, M. Legrand, Physically and geometrically non-linear vibrations of thin rectangular plates, Int. J. Non-Linear Mech. 58 (2014) 30–40.
[19] I.D. Breslavsky, M. Amabili, M. Legrand, Nonlinear vibrations of thin hyperelastic plates, J. Sound Vib. 333 (19) (2014) 4668–4681.
[20] M. Amabili, P. Balasubramanian, I. Breslavsky, G. Ferrari, R. Garziera, K. Riabova, Experimental and numerical study on vibrations and static deflection of a thin hyperelastic plate, J. Sound Vib. 385 (2016) 81–92.
[21] H.B. Khaniki, Hyperelastic structures: A review on the mechanics and biomechanics, Int. J. Non-Linear Mech. 148 (2023) 104–275.
[22] T. Sussman, K.J. Bathe, A finite element formulation for nonlinear incompressible elastic and inelastic analysis, Comput. Struct. 26 (1) (1987) 357–409.
[23] I. Babuška, M. Suri, Locking effects in the finite approximation of elasticity problems, Numer. Math. 62 (1992) 439–463.
[24] I. Babuška, M. Suri, On locking and robustness in the finite element method, SIAM J. Numer. Anal. 29 (1992).
[25] I. Caylak, R. Mahnken, Stabilization of mixed tetrahedral elements at large deformations, Internat. J. Numer. Methods Engrg. 90 (2) 218–242.
[26] A. Düster, S. Hartmann, E. Rank, p-FEM applied to finite isotropic hyperelastic bodies, Comput. Methods Appl. Mech. Engrg. 192 (47) (2003) 5147–5166.
[27] W. Chen, L. Wang, Large bending deformation of a cantilevered soft beam under external load: The applicability of inextensibility assumption of the centerline, Curr. Mech. Adv. Mater. 01 (2020).
[28] Y. Chen, L. Jin, Snapping-back buckling of wide hyperelastic columns, Extreme Mech. Lett. 34 (2020) 100600.
[29] M. Amabili, I.D. Breslavsky, J.N. Reddy, Nonlinear higher-order shell theory for incompressible biological hyperelastic materials, Comput. Methods Appl. Mech. Engrg. 346 (2019) 841–861.
[30] H.M. Verhelst, M.M. Möller, H.J. den Besten, A. Mantzaflaris, M.L. Kaminski, Stretch-based hyperelastic material formulations for isogeometric Kirchhoff-Love shells with application to wrinkling, Comput.-Aided Des. 139 (103075) (2021).
[31] R. Hassani, R. Ansari, H. Rouhi, Large deformation analysis of 2D hyperelastic bodies based on the compressible nonlinear elasticity: A numerical variational method, Int. J. Non-Linear Mech. 116 (2019) 39–54.
[32] E. Carrera, M. Cinefra, M. Petrolo, E. Zappino, Finite element analysis of structures through unified formulation, 2014.
[33] E. Carrera, E. Zappino, Carrera unified formulation for free-vibration analysis of aircraft structures, AIAA J. 54 (2015) 1–13.
[34] B. Wu, A. Pagani, M. Filippi, W.Q. Chen, E. Carrera, Large-deflection and post-buckling analyses of isotropic rectangular plates by Carrera Unified Formulation, Int. J. Non-Linear Mech. 116 (2019) 18–31.
[35] A. Pagani, E. Carrera, Unified one-dimensional finite element for the analysis of hyperelastic soft materials and structures, Mech. Adv. Mater. Struct. (2021) 1–14.
[36] P.J. Flory, Thermodynamic relations for high elastic materials, Trans. Faraday Soc. 57 (1961) 829–838.
[37] E. Karabelas, G. Haase, G. Plank, C. Augustin, Versatile stabilized finite element formulations for nearly and fully incompressible solid mechanics, Comput. Mech. 65 (2020) 1–23.
[38] S. Doll, K. Schweizerhof, On the development of volumetric strain energy functions, J. Appl. Mech. 67 (1999) 17–21.
[39] S.K. Melly, L. Liu, Y. Liu, J. Leng, A review on material models for isotropic hyperelasticity, Int. J. Mech. Syst. Dyn. 1 (1) 71–88.
[40] G.A. Holzapfel, Nonlinear Solid Mechanics: A Continuum Approach for Engineering, second print ed., John Wiley and Sons, Chichester, West Sussex, England, 2001.
[41] A. Pagani, E. Carrera, Unified formulation of geometrically nonlinear refined beam theories, Mech. Adv. Mater. Struct. 25 (1) (2018) 15–31.
[42] R. Borst, M. Crisfield, J. Remmers, C. Verhoosel, Non-Linear Finite Element Analysis of Solids and Structures, Second ed., 2012.
[43] R. Ansari, M.F. Oskouie, Rouhi, Nonlinear bending analysis of hyperelastic Mindlin plates: a numerical approach, Acta Mech. 232 (2021) 1–20.